A new methodology for a detailed investigation of quantized friction in ionic liquids

Romain Lhermerout, Susan Perkin

PCCP

ARTICLE TYPE

Cite this: DOI: 00.0000/xxxxxxxxxx

A new methodology for a detailed investigation of quantized friction in ionic liquids†

Romain Lhermerout* and Susan Perkin*

Received Date
Accepted Date

DOI: 00.0000/xxxxxxxxxx

When confined at the nanoscale between smooth surfaces, an ionic liquid forms a structured film responding to shear in a quantized way, i.e. with a friction coefficient indexed by the number of layers in the gap. So far, only a few experiments have been performed to study this phenomenon, because of the delicate nature of the measurements. We propose a new methodology to measure friction with a Surface Force Balance, based on the simultaneous application of normal and lateral motions to the surfaces, allowing for a more precise, comprehensive and rapid determination of the friction response. We report on proof-of-concept experiments with an ionic liquid confined between mica surfaces in dry or wet conditions, showing the phenomenon of quantized friction with an unprecedented resolution. First, we show that the variation of the kinetic friction force with the applied load for a given layer is not linear, but can be quantitatively described by two additive contributions that are respectively proportional to the load and to the contact area. Then, we find that humidity improves the resistance of the layers to be squeezed-out and extends the range of loads in which the liquid behaves as a superlubricant, interpreted by an enhanced dissolution of the potassium ions on the mica leading to a larger surface charge. There, we note a liquid-like friction behavior, and observe in certain conditions a clear variation of the kinetic friction force over two decades of shearing velocities, that does not obey a simple Arrhenius dynamics.

1 Introduction

Lubrication consists in inserting a substance -generally a liquid- between two solid surfaces in order to produce a controlled and stable friction. Its study is an old but still active field of research, because of the complexity of the phenomena at play[1,2]. As most real surfaces are rough, the contact between two macroscopic bodies involve in fact many mesoscopic asperities. A first consequence is that very large pressures, shear stresses and temperatures can be reached locally to promote tribological processes like wear, phase transitions or (electro)chemical reactions, making the role of the lubricant really challenging. A second consequence is that the lubricant should act at different scales simultaneously: for thick films, friction is governed by continuum hydrodynamics and depends on the lubricant viscosity (hydrodynamic regime); for thin films, friction is determined by subtle mechanisms at the molecular scale and depends on the lubricant chemical structure and its interactions with the solid surfaces (boundary lubrication regime). Ionics liquids, which are pure salts that are liquid at ambient temperature and pressure, are promising lubricants thanks to their unique physico-chemical stability[3]. During the last decade, many experiments with a Surface Force Apparatus/Balance (SFA/SFB) or an Atomic Force Microscope (AFM) have been performed to measure the normal interactions on a single asperity across an ionic liquid. They consistently showed the presence of a structural force, i.e. a force profile exhibiting a decaying oscillation, that has been attributed to the ordering of ions in the confined film, with a structure consisting of alternating layers of anions and cations (as sketched in Figure 1(a))[4–12]. Only a few studies have been conducted to measure the friction response in such structured film of ionic liquid, reporting on the phenomenon of "quantized friction", namely the fact that the friction coefficient is indexed by the number of layers composing the film[7,10,13–18]. Although the presence of such exotic behavior is now well-established experimentally, the fundamental mechanisms responsible for it are still debated. These outstanding questions motivate further detailed experimental investigations of quantized friction.

In this paper, we present a new methodology to measure friction in the boundary lubrication regime with a SFB. The principle consists in applying normal and lateral motions simultaneously -instead of alternatively- to the solid surfaces, allowing for a more precise, comprehensive and rapid determination of the friction-load relationship. First, we validate the method by measuring the

Department of Chemistry, Physical and Theoretical Chemistry Laboratory, University of Oxford, Oxford OX1 3QZ, UK. E-mail: romain.lhermerout@chem.ox.ac.uk; susan.perkin@chem.ox.ac.uk

† Electronic Supplementary Information (ESI) available. See DOI: 00.0000/xxxxxxxxxx/

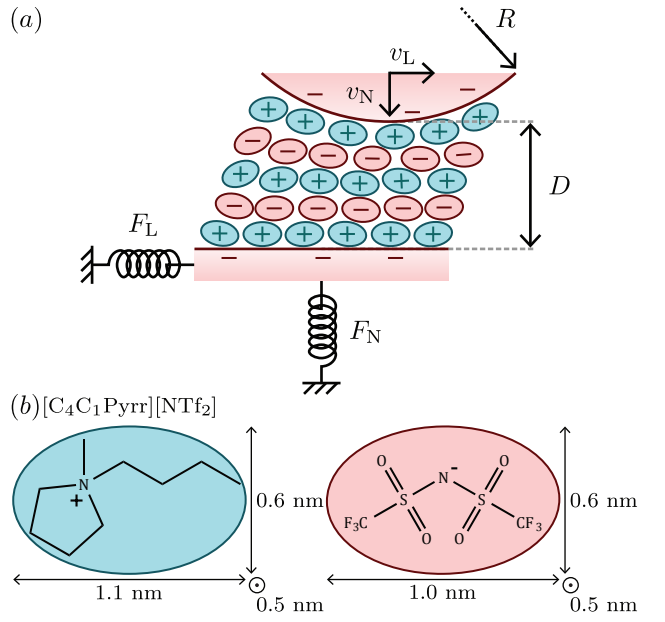

Fig. 1 (a) Schematic of the SFB experiment to measure interactions across a liquid (an ionic liquid in the present case) confined between two mica surfaces. The top surface is moved at normal velocity v_N and lateral velocity v_L, the bottom surface is mounted on springs to detect the normal force F_N and the lateral force F_L, the apical distance D and the radius of curvature R are measured by optical interferometry. (b) Chemical structure and sizes of $[C_4C_1Pyrr][NTf_2]$. Ion sizes are estimated from geometry, bond lengths and covalent radii, associated with the most stable configuration found by energy minimization (Chem3D 16.0, PerkinElmer Informatics).

phenomenon of quantized friction with an unprecedented resolution, for an ionic liquid confined between mica surfaces. This allows us to quantitatively explore the relationship between friction, load and contact area, as well as to elucidate the role of adhesion. Then, we show that traces of water induce an increase of the resistance of the layers to be squeezed-out, and an extension of the range of loads in which the liquid behaves as a superlubricant. There, we note a liquid-like friction behavior and observe that the kinetic friction force clearly depends on the shearing velocity, for a particular film composition in wet conditions. The dynamics is strongly non-linear, and is interpreted by means of different models of friction kinetics.

The paper is organised as follows. In section titled "Materials and Methods", we summarize the general procedure to perform a SFB experiment, and we present the new methodology to measure friction. In section titled "Results and Discussion", we describe and interpret the normal and lateral forces measurements performed across an ionic liquid, for different conditions of humidity and variable shearing velocities.

2 Materials and Methods

2.1 Surface Force Balance

The way the Surface Force Balance (SFB) works has been explained in details in previous publications[19–22]. Here we briefly recall the principle of the instrument, illustrated in Figure 1(a), and the details particular to the present experiments.

Muscovite mica is cleaved to produce atomically-smooth facets of micrometric thickness and millimetric extension, that are back-silvered and glued onto glass (fused silica) cylindrical (radius $R \sim 1$ cm) lenses with an epoxy resin (EPON 1004, Shell Chemicals). Two surfaces are made with mica of the same thickness, and are arranged in a cross-cylinder geometry. First, calibrations are done in a dry atmosphere, which is achieved by inserting P_2O_5, phosphorus pentoxide (Sigma-Aldrich, 99%), in the chamber and purging the chamber with N_2, nitrogen, for about one hour prior to the calibrations. The undeformed mica thickness $e_{\text{mica},0} = 7.431\ \mu$m is determined when the surfaces are in direct contact, following a procedure detailed in[23]. Secondly, measurements are performed with an ionic liquid, $[C_4C_1Pyrr][NTf_2]$, 1-butyl-1-methylpyrrolidinium *bis*[(trifluoromethane)sulfonyl]imide (Iolitec, 99%), which chemical structure and sizes are indicated in Figure 1(b) (molar mass $M = 422.41$ g/mol, density $\rho = 1.405$ g/mL, refractive index $n = 1.422$ and dynamic viscosity $\eta = 74$ mPa.s at 25°C[24]). This liquid is hygroscopic, and we use it either in dry or wet conditions. Dry conditions are achieved by drying the liquid in a Schlenck line at 60°C and 5×10^{-3} mbar for $\sim$ 10 hours and by inserting it in the chamber just after, which contains P_2O_5 and is purged again with N_2 for about one hour prior to the measurements. Such procedure is known to produce water content typically $\lesssim 100$ ppm[11,15,25]. Wet conditions are achieved by simply letting the ionic liquid equilibrate with ambient atmosphere during several days before the experiment and by inserting it in the chamber, which does not contain any desiccant and is filled with ambient air. In this case, the water content corresponds to the thermodynamic equilibrium of the ionic liquid with ambient humidity ($\sim 50\%$).

White light is passed through the confined medium, interferes in this optical resonator, and is then directed towards a spectrometer and collected by a CCD camera. The analysis of the Fringes of Equal Chromatic Order (FECO) then allows one to deduce the apical distance D, the contact radius a (when the surfaces are flattened) and the radius of curvature R[26]. In a separate paper[23], we show that the mica can be significantly compressed and that D incorporates the variations of thicknesses of the mica layers and of the liquid film, i.e the materials separating the two silver mirrors. For small changes of D, it is not possible to disentangle the contributions coming from the mica (indentation $2e_{\text{mica},0} - 2e_{\text{mica}} = 2\delta e_{\text{mica}}$, defined positive for compression and negative for dilatation) and the liquid (thickness D_{liquid}) with the FECO. In fact, we effectively measure the distance between the silver mirrors $D_{\text{mirrors}} = D_{\text{liquid}} + 2e_{\text{mica}}$, from which we subtract the undeformed mica thickness $2e_{\text{mica},0}$ calibrated in dry atmosphere, to finally obtain:

$$D = D_{\text{mirrors}} - 2e_{\text{mica},0} = D_{\text{liquid}} - 2\delta e_{\text{mica}}\ . \qquad (1)$$

D is measured with a precision of 0.02 nm given by the standard deviation of the signal, and an accuracy of 1 nm due to light disalignment when changing the contact spot[27]. As the glue thickness is heterogeneous, the top mica surface has a different curvature than the bottom glass lens, which has to be measured every time the contact spot is changed. The radius of curvature R as-

sociated to each measurement is indicated in the figure caption, and is known with an uncertainty of ~ 0.01 cm (mainly caused by the fact that the separation profile between the surfaces is observed up to a maximum scale ~ 50 nm $\ll R \sim 1$ cm). The contact radius a is measured with a precision of $0.03\ \mu$m given by the standard deviation of the signal, and an accuracy of $1\ \mu$m due to the uncertainty on the value of R, following a procedure explained in details in [23].

The top surface can be moved normally with a stepper motor (large displacement range $\sim 10\ \mu$m, poor linearity, mechanical vibrations induced), and also normally and laterally thanks to a sectored piezoelectric tube (small displacement range $\sim 1\ \mu$m, good linearity, no measurable mechanical vibrations induced). For a given run, the velocity v can be determined with a precision of $\sim 1\%$. From run to run, this velocity can typically vary by $\sim 10\%$ for the same control parameters, because of thermal drifts. In the following, some graphs result from the superposition of several runs, that is why the indicated velocities have to be associated with an error bar of $\sim 10\%$. The bottom lens is mounted on two springs: a normal (resp. lateral) spring of constant $k_N = 2670 \pm 84$ N/m (resp. $k_L = 379 \pm 2$ N/m), which is calibrated before the experiment by measuring its deflection (resp. its resonance frequency) when adding different masses. The normal force F_N is deduced from the temporal evolution of the distance $D(t)$ when applying a constant normal velocity v_N to the top surface, using a procedure that takes into account the viscous force that is not negligible at large separations (detailed in [22]). The lateral force F_L is directly measured with a capacitance probe when applying a constant lateral velocity v_L to the top surface, with a sensitivity of $\sim 10^{-3}$ mN. In comparison to previous studies performed in our group, the normal spring is here about 20 times stiffer, in order to apply larger loads (at fixed displacement range). Together with the stepper motor, it enables the identification of the first layer consisting of a monolayer of cations (labelled $i = 1$, as sketched in inset of Figure 2(a)), and the assessment of the resistance of the liquid to be squeeze-out under very large pressures. Together with the sectored piezoelectric tube, it enables one to reach the first layer of ions and so to explore the whole friction-load relationship with the new methodology (procedure detailed in next subsection). This comes with a price in terms of sensitivity limit for the normal force, $\sim 10^{-2}$ mN, which does not allow the detection of the anomalously long-range electrostatic force that has been observed with concentrated electrolytes [11,22,25,28–34].

The SFB is therefore a tool of choice to study the molecular mechanisms of friction: the two atomically-smooth surfaces are in contact on a single asperity (pure boundary lubrication regime), the apical distance D is measured with a resolution better than the molecular scale, and the geometry can be characterized *in-situ* (radius of curvature R, contact radius a). In the literature, the measured normal force F_N is generally rescaled by the radius of curvature R to compute an equivalent surface energy F_N/R, considering that mechanical deformations are negligible and that the Derjaguin approximation applies [19]. In the opposite case when the surfaces are strongly flattened, it is reasonable to assume that the total force F_N is mainly due to the interaction ion the flattened region, and so to rescale it by the contact area πa^2 to compute the local pressure $F_N/(\pi a^2)$. In this study, we explore a broad range of situations from no deformation to strong deformations, that is why we have chosen to simply use the force F without any rescaling in the plots.

2.2 New Methodology for friction measurement

So far, friction measurements with the SFA/SFB or the AFM were performed by applying normal and lateral motions alternatively: the surfaces were approached/retracted at a given distance under a given load, then the liquid was sheared, and so on [13,15]. The principle of the new methodology consists in applying normal and lateral motions simultaneously to the surfaces: if the approach/retraction rate is much smaller than the shearing rate (typically $v_N \sim 1$ nm/s $\ll v_L \sim 100$ nm/s), the distance and the load can be considered as constant within one shearing period. Such procedure has been already used by Hoth et al. [10] with a AFM but without analyzing the data to deduce the friction-load relationship, and by Crespo et al. [35] and us [36] with a SFA but not in the context of a structured liquid film.

Simply imposing a continuous instead of stepped motion in the normal direction potentially offers significant advantages. (i) The measurements are more precise (i.e. less scattered), because less time is left for the system to drift between points (inevitable long-term drifts due to thermal expansion and creep of the mechanical parts), which is necessary to investigate quantitatively the relationship between friction, load and contact area, and to finely test proposed models. (ii) The method allows for a more comprehensive exploration of friction-load relationship, in particular in the vicinity of spring instabilities (jump-out on retraction, jump-in on approach), which is crucial to elucidate the role of adhesion on friction, and to better understand the film dynamics during the squeeze-out transition. (iii) The whole friction phenomenology can be acquired more rapidly (in typically ~ 1 h instead of ~ 10 h to probe all the layers of a structured film), which is convenient to efficiently probe various physico-chemical systems and to assess the reproducibility of the measurements.

However, a careful implementation of the technique is required to avoid possible artefacts. First, the liquid structure itself can be affected by the shearing motion, a phenomenon that has been qualitatively interpreted as a combing of long-chain molecules [37–42]. Secondly, the friction force can be reduced by mechanical vibrations (potentially induced by the simultaneous normal motion), which qualitatively act as an effective temperature that helps to overcome the energy barrier associated with the molecules passing each other [43–48]. For the experiments reported in this paper, we ruled out these artefacts by systematically checking that the normal force profile is the same with a zero and non-zero lateral velocity (see Supplementary Figure 1), and that the friction-load relationship is the same with a zero and non-zero normal velocity (see Supplementary Figure 2).

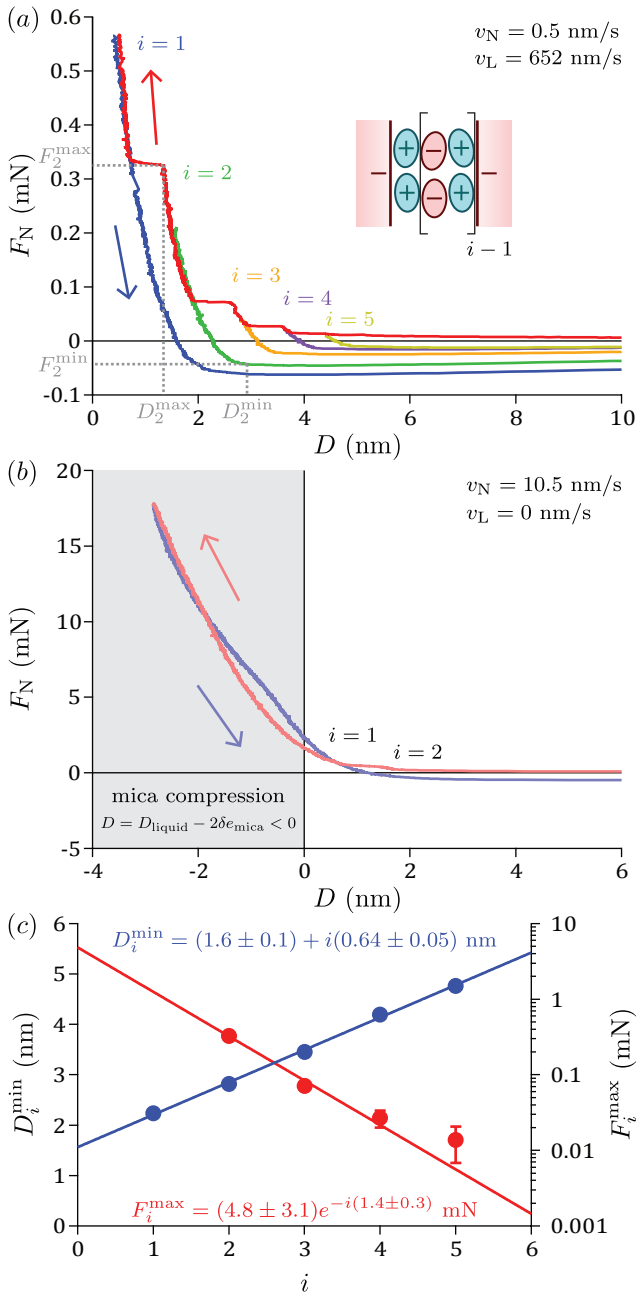

Fig. 2 Measurements for dry $[C_4C_1Pyrr][NTf_2]$ ($R = 0.92$ cm). (a) Normal force profile when moving the top surface with the piezoelectric tube at a normal velocity $v_N = 0.5$ nm/s and a lateral velocity $v_L = 652$ nm/s, showing structuring with 5 distinguishable layers labeled by i. For clarity, only the full approach is shown (in red), together with retractions from layers $i = 1$ (in blue), $i = 2$ (in green), $i = 3$ (in orange), $i = 4$ (in purple), $i = 5$ (in yellow). Inset: proposed structure of alternating layers of cations and anions. (b) Normal force profile when approaching (in faded red) or retracting (in faded blue) the top surface with the stepper motor at $v_N = 10.5$ nm/s. Negative distances D are reached at large loads, because the compression of mica exceeds the liquid thickness: $D = D_{liquid} - 2\delta e_{mica} < 0$[23].. The curves measured on approach and retraction in layer $i = 1$ are not perfectly superimposed because of mechanical imperfections of the set-up (poor linearity of the stepper motor, tiny rotations of the solids, etc.). (c) Distances D_i^{min} at the points of minimum force, as a function of the layer index i, in lin-lin representation (in blue); forces F_i^{max} at the points of maximum force, as a function of the layer index i, in log-lin representation (in red). Straight lines are the corresponding linear and exponential fits (equations 2 and 3).

3 Results and Discussion

3.1 Normal force

We begin with presenting measurements of the normal interaction force. Figure 2(a) shows the normal force profile obtained when moving the top surface with the piezoelectric tube at a normal velocity $v_N = 0.5$ nm/s and a lateral velocity $v_L = 652$ nm/s across dry $[C_4C_1Pyrr][NTf_2]$. When the ionic liquid is confined at the nanoscale, a structural force profile is observed, with five distinguishable layers labeled by i. Such structural force has been observed many times with ionic liquids, and attributed to the ordering of ions in the film, with a structure consisting of alternating layers of anions and cations (as sketched in inset)[4–12]. Because of the spring instability, the surfaces experience a jump-in on approach every time a layer is squeezed-out, and a jump-out on retraction from a given layer. Therefore several runs were in fact necessary for the most comprehensive exploration of the force profile. Supplementary Figure 3 shows the force profiles measured when approaching the top surface up to a given layer and retracting from this layer. From run to run, the whole force profile randomly shifts laterally by a fraction of nanometer. As the jump-in distances and the forces are reproducible, we consider that these shifts are non physical, but result from imperfections of the set-up like tiny rotations of the solids. That is why we have shifted manually the force profiles such that all the approaches are superimposed on the approach up to layer $i = 1$ (in red). Figure 2(a) shows the resulting force profile, with for clarity only the approach up to layer $i = 1$ (in red), and the retractions from the different layers ($i = 1$ in blue, $i = 2$ in green, $i = 3$ in orange, $i = 4$ in purple, $i = 5$ in yellow).

In a separate paper[23], we show that the oscillation due to local variations of liquid density in the confined film is in general convoluted with the mechanical response of the confining solids. For the system studied here, we found that (i) mica compression dominates liquid compression, i.e. the change of D within each layer is mainly due to the indentation of mica; (ii) contact mechanics is well described by the Derjaguin-Muller-Toporov (DMT) model[19,49–52], in particular the indentation of the solids is zero at the minimum force (jump-out point) and continuously increases up to the maximum force (jump-in point). For each layer i, we have measured the distance D_i^{min} at the point of minimum force (jump-out, as indicated in Figure 2(a) for $i = 2$), which does not include any influence of the mica compression. The variation of the distance D_i^{min} with the layer index i is shown in Figure 2(c), and exhibits a good linearity. It is fitted with the relation:

$$D_i^{min} = D_0^{min} + i\lambda^{min}, \qquad (2)$$

where the slope $\lambda^{min} = 0.64 \pm 0.05$ nm represents the mean layer thickness and the intersect $D_0^{min} = 1.6 \pm 0.1$ nm corresponds to the position of the extrapolated layer $i = 0$. Another method consists in measuring the average jump-in distance, supposing an unchanged mica compression and a fast viscous relaxation during the squeeze-out events, and providing a consistent value of 0.64 ± 0.01 nm for the mean layer thickness. Interestingly, this value is smaller than the mean ion pair diameter of 0.79 nm (given

by $\left(\frac{M}{\rho N_A}\right)^{1/3}$ with M the molar mass of the ionic liquid, ρ its bulk density and N_A the Avogadro's number[4]), perhaps suggesting a denser packing of ions in confinement than in the bulk. However, our value is also smaller than the previous measurements performed with the same ionic liquid, reporting a mean layer thickness of 0.80 ± 0.04 nm between two mica surfaces with a SFB[53] and 0.79 nm between a mica surface and a Si_3N_4 tip with an AFM[54]. A possible explanation for this difference is the inherent contribution from viscosity to the force profile, in particular in vicinity to a spring instability. For the method using the distances $D_i^{\min}$ at the points of minimum force (giving a mean layer thickness of 0.64 ± 0.05 nm), viscosity tends to move the minima towards larger distances, even more than adhesion is larger (i.e. smaller layer index i). For the method using the jump-in distances (giving a mean layer thickness of 0.64 ± 0.01 nm), viscosity tends to reduce the size of the jumps. In both cases, viscous effects possibly lead to an underestimation of the mean layer thickness. Previous studies may be less affected by viscosity, as retractions were performed by slow steps in the SFB study[53] (with similar radius of curvature), and the radius of curvature was six orders of magnitude smaller in the AFM study[54] (with a velocity less than an order of magnitude larger). Therefore, applying a stepped motion is preferable to a continuous motion in order to accurately determine the mean layer thickness.

An important aspect to interpret the structural force profiles is to identify the composition of the layers. As the period is similar to the mean ion pair diameter, it is qualitatively considered that one squeeze-out event corresponds to the squeeze-out of an electroneutral "slab" of one cation layer and one anion layer. In the case of negatively charged surfaces, the first layer ($i = 1$) is then assumed to be composed of a monolayer of cations (as sketched in inset of Figure 2(a)). Direct solid-solid contact is never reached, because of the strong electrostatic attraction between the cations and the negatively charged surfaces. For our experiment, one can ask whether we really reach this single layer of cations within the explored range of loads. The position of the first layer at the point of minimum force (including no indentation of the surfaces) is $D_1^{\min} = 2.2 \pm 1.0$ nm, a bit larger than the cation sizes (given in Figure 1(b)). However, the measurement of the absolute distance D depends on many delicate steps (alignment of the optics, calibration of the mica thickness in dry atmosphere, choice of a particular run to shift the force profiles laterally), and deducing the thickness of the monolayer from the cation sizes requires to know their conformations, making accurate comparisons difficult. For each layer i, we have measured the force $F_i^{\max}$ at the point of maximum force (jump-in, as indicated in Figure 2(a) for $i = 2$). The variation of the distance $F_i^{\max}$ with the layer index i is shown in Figure 2(c) in log-lin representation, and exhibits a good linearity. It is fitted with the relation:

$$F_i^{\max} = F_0^{\max} \exp\left(-i \frac{\lambda^{\max}}{\zeta^{\max}}\right), \qquad (3)$$

where the slope gives access to the ratio $\frac{\lambda^{\max}}{\zeta^{\max}} = 1.4 \pm 0.3$ of the period of the oscillation on the decay length (i.e. typical distance from a surface on which the oscillations of local liquid density are damped), and the intersect corresponds to the amplitude $F_0^{\max} = 4.8 \pm 3.1$ mN of the extrapolated layer $i = 0$. If we extrapolate this fit to the layer $i = 1$, it predicts that the next squeeze-out event would take place at a force $F_N = 1.3 \pm 0.6$ mN. Figure 2(b) shows the normal force profile obtained when approaching (in faded red) then retracting (in faded blue) the top surface with the stepper motor at a velocity $v_N = 10.5$ nm/s. We do not observe any additional jump-in for a force up to $F_N = 17.80$ mN. Thus, we think that the layer seen at the maximum load is indeed composed of a single layer of cations, and we identify it as $i = 1$. Note that negative distances D are reached at large loads, because the compression of mica exceeds the liquid thickness: $D = D_{\text{liquid}} - 2\delta e_{\text{mica}} < 0$[23].

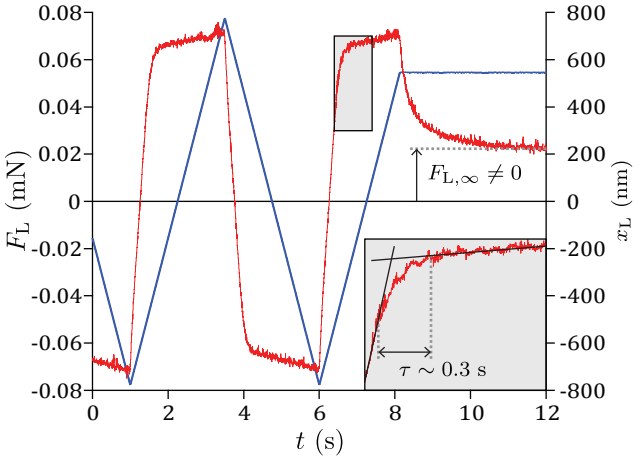

Fig. 3 Measurements for wet $[C_4C_1Pyrr][NTf_2]$ ($R = 1.45$ cm), at fixed load $F_N = 2.79$ mN, distance $D = -1.05$ nm (where $D = D_{\text{liquid}} - 2\delta e_{\text{mica}} < 0$) and contact radius $a = 12.86$ μm in layer $i = 2$. Temporal evolutions of the lateral displacement x_L and lateral force F_L, showing a liquid-like friction behavior. Inset: zoom on a part of the signal, delimited by a gray rectangle in the main graph. The tiny oscillation is due to the resonance of the mass-spring system at ~ 20 Hz.

On a practical point of view, we observe that applying a maximum load $F_N = 17.80$ mN does not lead to a complete squeeze-out of the confined liquid film, even if the confining solids are already strongly deformed: mica is compressed by a few nanometers and the surfaces are flattened on a contact radius $a = 21.61$ μm, corresponding to a pressure $\sim F_N/(\pi a^2) \sim 12$ MPa. The first layer, which consists of a monolayer of cations, is so strongly bounded to the oppositely charged mica surfaces that it is never squeezed-out. This is a very good property for a potential lubricant, because keeping the solid surfaces apart is an efficient way to prevent wear.

3.2 Lateral force

In this subsection, we identify the nature of the friction response, by analyzing the shape of the lateral force when the liquid film is sheared under constant conditions in the normal direction. Figure 3 shows the temporal evolutions of the lateral displacement x_L and lateral force F_L for wet $[C_4C_1Pyrr][NTf_2]$, at fixed load $F_N = 2.79$ mN, distance $D = -1.05$ nm (where $D = D_{\text{liquid}} - 2\delta e_{\text{mica}} < 0$) and contact radius $a = 12.86$ μm in layer $i = 2$. When

starting to apply a constant lateral velocity $v_L = 639$ nm/s, the lateral force exhibits first a linear variation of slope $k_L \times v_L$, then a relaxation with a typical timescale $\tau \sim 0.3$ s, there a smooth-sliding creep of amplitude ~ 0.07 mN. When the direction of the motion is reversed, the lateral force responds in a symmetric manner with respect to the horizontal axis. If the lateral motion is suddenly stopped, the lateral force exhibits a relaxation with a similar timescale τ towards an amplitude $F_{L,\infty} \neq 0$.

To interpret the observed friction behavior, we first recall the response of a simple viscous liquid (bulk viscosity $\eta = 74$ mPa.s) sheared between two planar surfaces (liquid thickness $D_{liquid} \sim 1$ nm, area $\mathscr{A} \sim \pi a^2 \sim 523\ \mu m^2$), the top one being moved at a lateral velocity $v_L = 639$ nm/s and the bottom one being attached to a lateral spring of stiffness $k_L = 379$ N/m[20,37]. For a charge-less, Newtonian liquid in an incompressible and laminar flow between undeformable surfaces with a no-slip boundary condition, the force opposing the motion is purely viscous and results from the Couette flow in the gap. If the inertial term is negligible in the equation of motion for the bottom surface, the temporal evolution of the lateral force is given by the balance of the viscous force and the restoring spring force. When starting to apply a constant lateral velocity $v_L = 639$ nm/s, classical hydrodynamics predicts that the lateral force exhibits first a linear variation of slope $k_L \times v_L$, then an exponential relaxation with a timescale $\frac{\mathscr{A}\eta}{k_L D_{liquid}} \sim 10^{-4}$ s, there a smooth-sliding plateau of amplitude $\frac{\mathscr{A}\eta v_L}{D_{liquid}} \sim 2 \cdot 10^{-5}$ mN. When the direction of the motion is reversed, the lateral force responds in a symmetric manner with respect to the horizontal axis. If the lateral motion is suddenly stopped, the lateral force exhibits an exponential relaxation with the same timescale towards a zero amplitude. Therefore, the phenomenology obtained in our experiment is qualitatively similar to the one expected for a simple viscous liquid, but with three important differences: (i) the forces and timescales involved are more than three orders of magnitude larger, (ii) there is creep instead of a plateau, (iii) a non-zero force is sustained after stopping the motion. That is why the response measured here is identified as a liquid-like friction behavior[37]. In past experiments with the same ionic liquid a friction response with features typical of solid-like behavior has been observed. In the Supplementary Material we discuss in detail the possible origin of this difference, and conclude that relative mica orientation (twist angle) is most likely to be the underlying cause.

3.3 Friction-Load relationship

In this subsection, we use the new methodology to explore the friction-load relationship for dry $[C_4C_1Pyrr][NTf_2]$. Figure 4(a) shows the temporal evolutions of the apical distance D and lateral force F_L, when moving the top surface with the piezoelectric tube at a normal velocity $v_N = 0.5$ nm/s and a lateral velocity $v_L = 652$ nm/s. The amplitude of the lateral force is below the sensitivity limit of $\sim 10^{-3}$ mN before reaching layer $i = 2$, then very small but discernible in this layer, and finally larger in layer $i = 1$. In the inset of Figure 4(a) is plotted the variation of the lateral force during the squeeze-out transition from layer $i = 2$ to layer $i = 1$, a measurement that is possible with the new methodology. The apical distance varies by ~ 0.64 nm in ~ 10 s, during which about four shearing cycles are performed. In this particular case, we are in fact probing the friction response of a transient film configuration, integrated over a time ~ 2.5 s. The amplitude of the lateral force increases continuously during the squeeze-out transition, showing that an heterogeneous film composed of a mixture of $i = 2$ and $i = 1$ areas gives a friction response that is intermediate between the responses of homogeneous $i = 2$ or $i = 1$ films.

To analyze quantitatively the large amount of data generated by this new methodology, we have written a simple code. For each shearing period, it automatically extracts the average lateral force during the creep stage, identified as the kinetic friction force $F_{L,k}$, as well as the average load F_N, apical distance D and contact radius a. We have done this for all the runs that were necessary for the most comprehensive exploration of the structural force profile (see for example Supplementary Figure 4, that shows the full temporal evolutions of the apical distance D and lateral force F_L during the approach up to layer $i = 1$ and the retraction from this layer). Figure 4(b) shows the kinetic friction force $F_{L,k}$ as a function of the load F_N, when moving the top surface with the piezoelectric tube at a normal velocity $v_N = 0.5$ nm/s and a lateral velocity $v_L = 652$ nm/s. The friction coefficient -evaluated as the slope in this friction-load representation- is clearly indexed by the number of ions composing the liquid film, which is the signature of the quantized friction phenomenon. This implies that friction is a multi-valued function of the load. In layer $i = 2$ (retraction branch in green), the friction coefficient is $\mu_2 = 0.0064 \pm 0.0006$, i.e. the film composed of two cations layers plus one anions layer behaves as a superlubricant (conventionally defined by a kinetic friction coefficient < 0.01[2]). In layer $i = 1$ (retraction branch in blue), the friction coefficient is $\mu_1 = 0.210 \pm 0.003$ (almost two orders of magnitude larger!), i.e. the film composed of a monolayer of cations behaves as a poor lubricant. The transition between the two regimes happens at a load $F_N = 0.33$ mN, corresponding to a pressure $\sim F_N/(\pi a^2) \sim 2$ MPa (given a contact radius $a = 6.45\ \mu$m).

In comparison to previous studies, the new methodology provides much less scattered data points. This allows us to quantitatively tests different empirical laws of friction, that we briefly recall in the following. For smooth adhering surfaces, it has been argued that the friction force $F_{L,k}$ should increase proportionally with the load F_N, i.e. $F_{L,k} = \mu(F_N - F^{min})$ (with μ the friction coefficient and F^{min} the adhesion force), due to the increase of the pressure in the film -the adhesion acting as an internal pressure-[55–58]. It has also been suggested that the friction force $F_{L,k}$ should increase proportionally with the contact area $\mathscr{A}$, i.e. $F_{L,k} = \sigma_c \mathscr{A}$ (with σ_c the critical shear stress), due to the increase of the surface on which shear stress is integrated[52,59–63]. More generally, it has been proposed that friction comes from these two contributions, i.e. $F_{L,k} = \mu F_N + \sigma_c \mathscr{A}$[64]. For the system studied here, we show in a separate paper[23] that contact mechanics is well described by the Derjaguin-Muller-Toporov (DMT) model[19,49–52]. The relation between the contact area and the load is $\mathscr{A} = \pi \left(\frac{R}{K}\right)^{2/3} \left(F_N - F^{min}\right)^{2/3}$, with R the radius of curvature and $K = 16.7 \pm 0.5$ GPa the fitted effective elastic modulus -the adhesion again acting as an internal pressure-. Finally, we

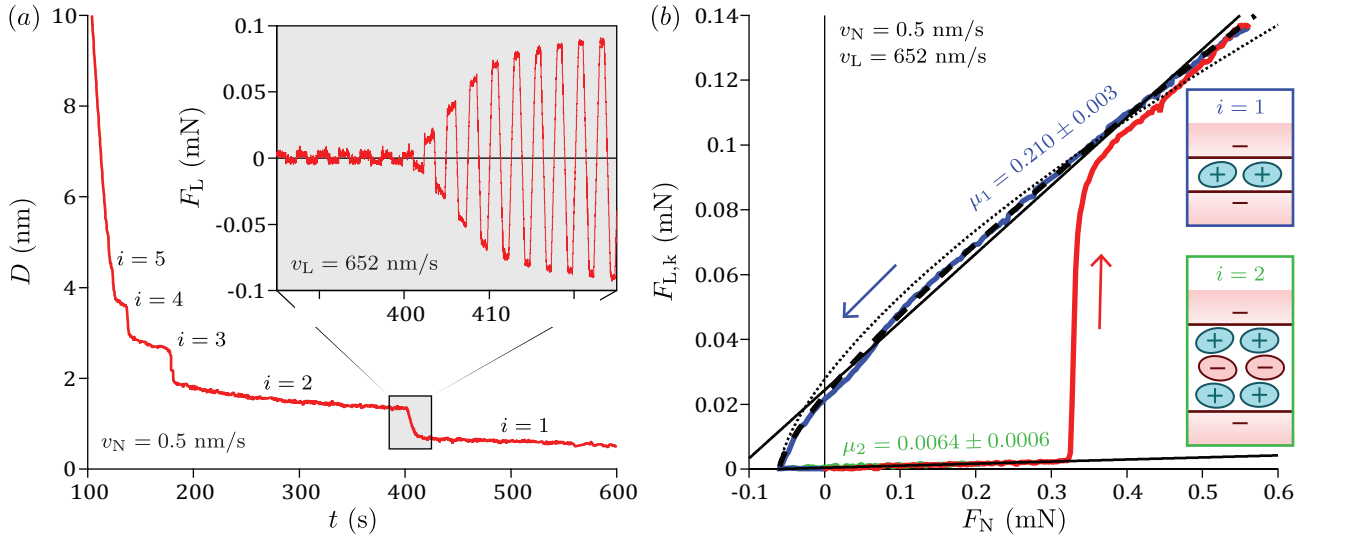

Fig. 4 Measurements for dry $[C_4C_1Pyrr][NTf_2]$ ($R = 0.92$ cm), when moving the top surface with the piezoelectric tube at a normal velocity $v_N = 0.5$ nm/s and a lateral velocity $v_L = 652$ nm/s. (a) Temporal evolution of the apical distance D on full approach. The inset shows the temporal evolution of the lateral force F_L during the squeeze-out transition from layer $i = 2$ to layer $i = 1$. (b) Kinetic friction $F_{L,k}$ as a function of load F_N on full approach (in red) then retraction from layer $i = 1$ (in blue). Friction is above the sensitivity limit for the layers $i = 1$ and $i = 2$ (proposed film structures in insets). Straight lines are fits with the left-hand term of equation 4, with $\{\mu_1 = 0.210 \pm 0.003, F_1^{\min} = -0.12 \pm 0.01$ mN$\}$ and $\{\mu_2 = 0.0064 \pm 0.0006, F_2^{\min} = -0.062 \pm 0.008$ mN$\}$. The dotted line is a fit for layer $i = 1$ with the right-hand term of equation 4, with $\{\sigma_{c,1} = 857 \pm 6$ kPa, $F_1^{\min} = -0.06$ mN$\}$. The dashed line is a fit for layer $i = 1$ with the whole equation 4, with $\{\mu_1 = 0.092 \pm 0.004$, $\sigma_{c,1} = 529 \pm 13$ kPa, $F_1^{\min} = -0.06$ mN$\}$.

fit the friction-load relationship in layer $i = 1$ with the following empirical law:

$$F_{L,k} = \mu_i \times \left(F_N - F_i^{\min}\right) + \sigma_{c,i} \times \pi \left(\frac{R}{K}\right)^{2/3} \left(F_N - F_i^{\min}\right)^{2/3}, \quad (4)$$

where μ_i, $\sigma_{c,i}$ and $F_i^{\min}$ are respectively the friction coefficient, critical shear stress and adhesion force associated with layer i. This equation gives $F_{L,k} = 0$ at $F_N = F_i^{\min}$, which is in agreement with our systematic observation that the friction force goes to zero at the jump-out point. If we suppose first that friction is purely load-controlled and we fit with the left-hand term of equation 4 only (straight line in Figure 4(b)), we get $\{\mu_1 = 0.210 \pm 0.003$, $F_1^{\min} = -0.12 \pm 0.01$ mN$\}$ (two free parameters). The fit is clearly not satisfactory and overestimate the adhesion force (compared to the directly measured $F_1^{\min} = -0.06$ mN), because it does not describe the significant concave curvature that is observed experimentally. If we suppose on the contrary that friction is purely contact area-controlled and we fit with the right-hand term of equation 4 only (dotted line in Figure 4(b)), we get $\{\sigma_{c,1} = 857 \pm 6$ kPa, $F_1^{\min} = -0.06$ mN$\}$ (one free parameter, the adhesion force being fixed). The fit is much better in the vicinity of the adhesion minimum, but now overestimates the concavity of the curve. In fact, the experimental data lie in between the two previous fits, and if we fit with the full equation 4 (dashed line in Figure 4(b)), we obtain a very good fit with $\{\mu_1 = 0.092 \pm 0.004$, $\sigma_{c,1} = 529 \pm 13$ kPa, $F_1^{\min} = -0.06$ mN$\}$ (two free parameters, the adhesion force being fixed).

To summarize, the measured friction-load relationship can be described quantitatively with an empirical law, providing that two additive contributions are included, the first proportional the load and the second proportional to the contact area. In the previous experimental studies of quantized friction across ionic liquids, the friction-load relationship was found to be compatible with a linear variation (i.e. a load-controlled friction), given the scattering on the data points [13,15]. It is thanks to the new methodology that we are able to measure the friction-load relationship with an unprecedented resolution, and to quantitatively test the different empirical laws of friction. This is crucial not only for a better understanding of the physics of friction in general, but also to extract quantities μ and σ_c that are intrinsic to the physico-chemical system used and not affected by the particular geometry of the experiment. Unfortunately, such high-resolution measurements are not always possible, for example when friction is small or varies slowly, or cannot be measured on a wide range of loads (like for layer $i = 2$ in Figure 4(b)). However, we note that the different fits in layer $i = 1$ provide friction coefficients of same order of magnitude. That is why we have decided to fit linearly the friction-load relationships measured with a low resolution, as a semi-quantitative evaluation of the lubrication performances.

3.4 Effect of humidity

In this subsection, we present an experiment performed with wet $[C_4C_1Pyrr][NTf_2]$, illustrating the versatility and the efficiency of the new methodology. The measurements, shown in Figure 5, are qualitatively similar to the dry case, in the sense that we also observe a structural force profile, a liquid-like friction behavior, and a quantized friction-load relationship. But important differences emerge when comparing the results quantitatively.

Figures 5(a) and 5(b) show the normal force profile obtained when moving the top surface normally with the piezoelectric tube at $v_N = 0.5$ nm/s or with the stepper motor at $v_N = 3.4$ nm/s

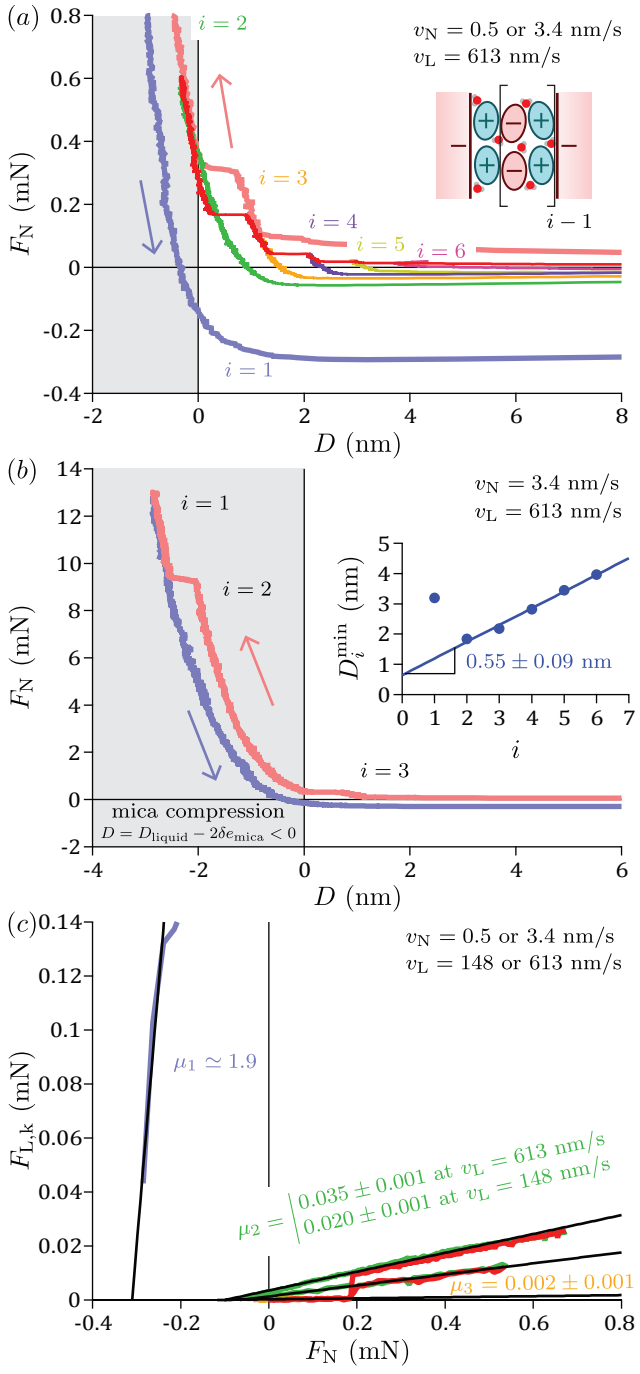

Fig. 5 Measurements for wet $[C_4C_1Pyrr][NTf_2]$ ($R = 1.45$ cm). (a) Normal force profile when moving the top surface normally with the piezoelectric tube at $v_N = 0.5$ nm/s or with the stepper motor at $v_N = 3.4$ nm/s (faded red and faded blue) and laterally at $v_L = 652$ nm/s, showing structuring with 6 distinguishable layers labeled by i. For clarity, only the two full approaches are shown (in red for the piezoelectric tube, in faded red for the stepper motor), together with retractions from layers $i = 1$ (in faded blue), $i = 2$ (in green), $i = 3$ (in orange), $i = 4$ (in purple), $i = 5$ (in yellow), $i = 6$ (in pink). Inset: proposed structure of alternating layers of cations and anions with water traces. (b) Normal force profile when approaching or retracting the top surface with the stepper motor at $v_N = 3.4$ nm/s. Inset: distances D_i^{min} at the points of minimum force, as a function of the layer index i, and corresponding linear fit (equation 2). (c) Kinetic friction $F_{L,k}$ as a function of load F_N. Straight lines are fits with the left-hand term of equation 4, with $\{\mu_1 \sim 1.9,\ F_1^{min} \sim -0.3$ mN$\}$, $\{\mu_2 = 0.035 \pm 0.001,\ F_2^{min} = -0.101 \pm 0.004$ mN$\}$ and $\{\mu_3 = 0.002 \pm 0.001,\ F_3^{min} = -0.12 \pm 0.03$ mN$\}$. Friction clearly depends on lateral velocity in layer $i = 2$, with $\{\mu_2 = 0.020 \pm 0.001,\ F_2^{min} = -0.07 \pm 0.01$ mN$\}$ at $v_L = 148$ nm/s. As retraction from $i = 1$ has been performed at a relatively large velocity, D_1^{min} and F_1^{min} are strongly affected by viscous effects, and μ_1 is estimated with only a few shearing periods.

and laterally at $v_L = 652$ nm/s. The wet ionic liquid gives rise to a structural force, with six distinguishable layers. The mean layer thickness is found to be 0.55 ± 0.09 nm by linearly fitting the variation of the distance D_i^{min} with the layer index i (see inset of Figure 5(b)), or 0.68 ± 0.16 nm by measuring the average jump-in distance. These values are close to the ones obtained in dry conditions, suggesting a picture of minority water molecules sitting between ions without disrupting the film structure (as sketched in inset of Figure 5(a)). Such scenario is consistent with a previous SFB study using different mixtures of $[C_4C_1Pyrr][NTf_2]$ and propylene carbonate[53], which showed that the period of the structural force undergoes an abrupt transition at a threshold ion concentration, i.e. that the mean layer thickness is basically determined by the majority compound. But our observation is in contrast with previous SFB/SFA experiments using $[C_{10}C_1Im][NTf_2]$, 1-decyl-1-methylpyrrolidinium *bis*[(trifluoromethane)sulfonyl]imide[17], or $[C_2C_1Im][FAP]$, 1-ethyl-3-methylimidazolium *tris*(pentafluoroethyl)trifluorophosphate[25], which reported on a dilation of the layers with humidity by respectively ~ 0.4 nm and ~ 0.2 nm (close to the water size estimated as $\left(\frac{M}{\rho N_A}\right)^{1/3} = 0.31$ nm, with $M = 18.02$ g/mol the molar mass of water, $\rho = 1$ g/mL its bulk density and N_A the Avogadro's number), interpreted by a segregation of the water molecules towards the polar moieties of ions. In fact, molecular dynamics simulations have shown that the influence of humidity on layer thickness depends on the shape of the ions and on the surface charge, and that the addition of water may even induce a thinning of the layers, attributed to an increase of the dielectric constant and so a reduction of the electrostatic interactions between the ions[65]. Returning to our measurements, we find that the amplitude of the structural force is much larger than in the dry case. Striking illustrations of this structural strengthening are the facts that a sixth layer can be detected, and that the squeeze-out transition from layer $i = 2$ to layer $i = 1$ happens at a very large load $F_N = 9.22$ mN (corresponding to a pressure $\sim F_N/(\pi a^2) \sim 8$ MPa, given a contact radius $a = 18.94$ μm), which can be reached within the range of the stepper motor only thanks to the choice of a large normal spring constant. In comparison with the dry case, this corresponds to a load ~ 28 times larger, or a pressure ~ 4 times larger. A similar behavior has been observed with SFA experiments using $[C_2C_1Im][NTf_2]$, 1-ethyl-3-methylimidazolium *bis*[(trifluoromethane)sulfonyl]imide[11]. Qualitatively, such amplification of the ion density oscillations can be attributed to an enhanced dissociation of the potassium ions on the mica, leading to a larger surface charge.

Figure 5(c) shows the kinetic friction force $F_{L,k}$ as a function of the load F_N for the wet ionic liquid. Again, the friction coefficient is indexed by the number of ions composing the liquid film, i.e friction is quantized. However, the lateral force is above the sensitivity limit for three layers, instead of two for the dry case. In layer $i = 3$ (retraction branch in orange), the friction coefficient is $\mu_1 = 0.002 \pm 0.001$, i.e. the film composed of three cations layers plus two anions layers behaves as an extremely good superlubricant. In layer $i = 2$ (retraction branch in green), the friction

coefficient is $\mu_2 = 0.035 \pm 0.001$, i.e. the film composed of two cations layers plus one anions layer is almost a superlubricant. For layer $i = 1$ (retraction branch in faded blue), the friction coefficient is $\mu_3 \sim 1.9$, i.e. the film composed of a monolayer of cations is a poor lubricant. Note that retraction from layer $i = 1$ has been performed at a relatively large velocity, so the value of μ_1 is estimated with only a few shearing periods. Supplementary Figure 2 shows the friction-load relationship that has been measured in a larger range of loads for layer $i = 2$, by approaching the surfaces by discrete steps with the stepper motor. Similarly to the dry case, a good fit can be achieved with equation 4, providing that the two contributions are included, the first proportional to the load and the second proportional to the contact area (with $\{\mu_2 = 0.0129 \pm 0.003,\ \sigma_{c,2} = 56 \pm 2$ kPa, $F_2^{\min} = -0.06$ mN$\}$).

Overall, humidity is found to strongly increase the resistance of the layers to be squeezed-out, without changing significantly their corresponding thicknesses and friction coefficients. Consequently, it leads to an extension of the range of loads in which the liquid behaves as a superlubricant. Such beneficial effect of water on the lubricating performances is extremely interesting for applications, given that ionic liquids are hygroscopic and that lubricated systems are never perfectly insulated from ambient moisture.

3.5 Kinetics aspects

In this subsection, we consider the influence of the shearing velocity on the friction force. Supplementary Figure 5 shows the friction-load relationships measured in dry conditions at $v_L =$ 652 nm/s and $v_L = 67.9$ nm/s. No clear trend is found within the experimental errors, whether in layer $i = 1$ or in layer $i = 2$. Figure 5(c) shows the friction-load relationships measured in wet conditions at $v_L = 613$ nm/s and $v_L = 148$ nm/s. In layer $i = 3$, no clear trend is found within the experimental errors, and layer $i = 1$ was explored at only one shearing velocity. In layer $i = 2$, however, the friction clearly depends on the shearing velocity. More precisely, the kinetic friction force goes to zero at the same adhesion minimum in both cases, but with a friction coefficient that is larger with the largest shearing velocity. These observations are consistent with previous SFB experiments performed with the same ionic liquid in our group, showing that in dry conditions the kinetic friction is independent of the shearing velocity in the range $v_L \in [200; 1000]$ nm/s, whatever the layer considered [15]. Our findings are also comparable with previous colloidal probe AFM experiments performed with protic ionic liquids (ethylammonium nitrate (EAN), propylammonium nitrate (PAN), ethylammonium formate (EAF), etc.) between a silica sphere ($R \sim 10$ μm) and a mica surface, reporting on an increase of the friction coefficient with the shearing velocity in the range $v_L \in [5000; 40000]$ nm/s, for some particular film compositions [13,14,16]. However, it is not clear why a dependence of the shearing velocity on the friction force is found or not, depending on the physico-chemical system and the layer considered.

To investigate this dynamics quantitatively, we have sheared the liquid under constant conditions in the normal direction, exploring two decades of lateral velocities. Figure 6(a) shows the lateral force F_L as a function of the lateral displacement x_L when shearing wet $[C_4C_1Pyrr][NTf_2]$ at different velocities $v_L \in \{32; 128; 639; 1918; 3197\}$ nm/s (with same displacement range), at fixed load $F_N = 2.79$ mN, distance $D = -1.05$ nm (where $D = D_{\text{liquid}} - 2\delta e_{\text{mica}} < 0$) and contact radius $a = 12.86$ μm in layer $i = 2$. A liquid-like friction behavior is obtained for all the friction loops, but with a kinetic friction force that increases monotonically with the the shearing velocity. Finally, Figure 6(b) shows the kinetic friction force $F_{L,k}$ as a function of the lateral velocity v_L, in lin-log representation (Supplementary Figures 6(a) and 6(b) show the same data, respectively in lin-lin and log-log representations). The dynamics is strongly non-linear, and is interpreted with different models of friction kinetics in the following.

In friction experiments between smooth surfaces, dynamics is generally found to be thermally-activated, i.e. obeying an Arrhenius law of the form:

$$F = F_0 \ln \frac{v}{v_0}. \tag{5}$$

Qualitatively, such thermally-activated dynamics is associated with the picture of molecules that must overcome energy barriers in order to pass each other, with the external force inducing a potential biais and with the temperature allowing for the crossing of non-zero barriers. It has been observed for dry friction (between Langmuir-Blodgett films with a SFA [66], between a NaCl surface and a silicon tip with an AFM [67]), as well as for lubricated friction in the boundary regime (between mica surfaces across apolar liquids or aqueous electrolytes with a SFA [68,69], between mica surface and silicon colloid across protic ionic liquids with a colloidal probe AFM [13,14,16]). We have fitted our data with equation 5 (red curve in Figure 6(b)), giving $\{F_0 = (23 \pm 4) \cdot 10^{-3}$ mN, $v_0 = 18 \pm 10$ nm/s$\}$. Clearly, an Arrhenius law does not provide a satisfactory fit of the dynamics measured over two decades of velocities in the range $v_L \in [30; 3000]$ nm/s, which exhibits a significant curvature in a lin-log representation. This is in contrast with the previous colloidal probe AFM studies of friction across ionic liquids [13,14,16], showing a dynamics compatible with an Arrhenius law over one decade of velocities in the range $v_L \in [5000; 40000]$ nm/s. A modified Arrhenius law has been proposed, in the case where the potential biais induced by the external force is so large that the energy barrier almost disappears (i.e. at the vicinity of the spinodal) [70–72]:

$$F = F_c - \Delta F \left(\ln \frac{v_c}{v} \right)^{2/3}. \tag{6}$$

Our data have been fitted with this model (green curve in Figure 6(b)), giving $\{F_c = 0.13 \pm 0.02$ mN, $v_c = (3.4 \pm 1.5) \cdot 10^3$ nm/s, $\Delta F = (36 \pm 7) \cdot 10^{-3}$ mN$\}$. It better reproduces the curvature of the data, and predicts that the spinodal transition is reached just at the top of the explored range of lateral velocities. However, several experimental, numerical and theoretical works in the literature propose to describe the lubricated friction dynamics by means of a shear-thinning rheology with an effective viscosity that decreases as ${v_L}^{-2/3}$, or equivalently a friction force that increases as ${v_L}^{1/3}$ [73–78]. This can be written as an empirical power-law of the form:

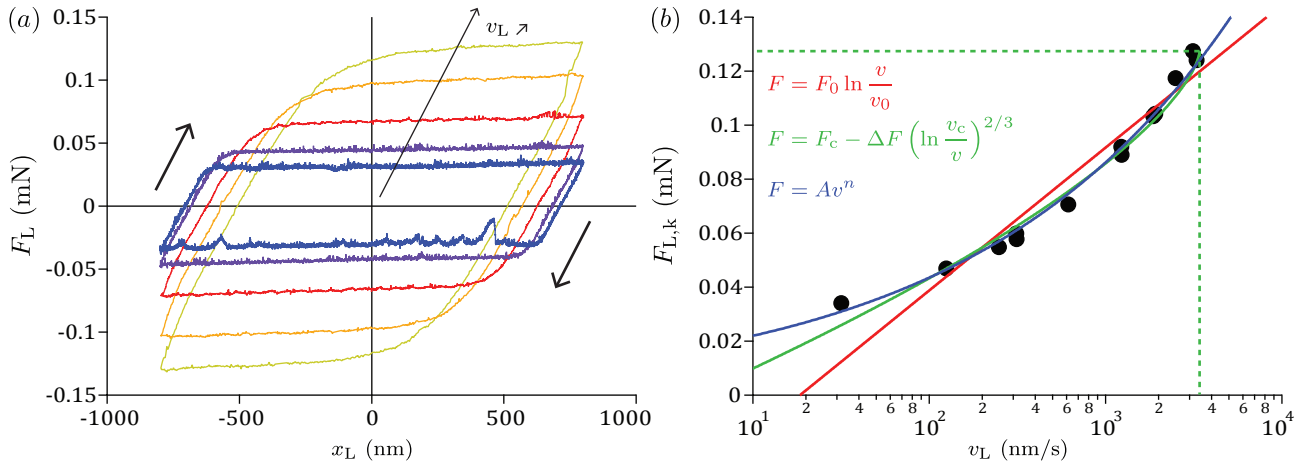

Fig. 6 Measurements for wet $[C_4C_1Pyrr][NTf_2]$ ($R = 1.45$ cm), at fixed load $F_N = 2.79$ mN, distance $D = -1.05$ nm (where $D = D_{liquid} - 2\delta e_{mica} < 0$) and contact radius $a = 12.86$ μm in layer $i = 2$. (a) Lateral force F_L as a function of lateral displacement x_L, for different lateral velocities $v_L \in \{32; 128; 639; 1918; 3197\}$ nm/s respectively in blue, purple, red, orange and yellow. The bumps on the signals, particularly visible for the blue curve, are due to external vibrations that are not totally suppressed by the damping elements of the SFB. (b) Kinetic friction $F_{L,k}$ as a function of lateral velocity v_L, in lin-log representation. The red curve is a fit with equation 5 giving $\{F_0 = (23 \pm 4) \cdot 10^{-3}$ mN, $v_0 = 18 \pm 10$ nm/s$\}$. The green curve is a fit with equation 6 giving $\{F_c = 0.13 \pm 0.02$ mN, $v_c = (3.4 \pm 1.5) \cdot 10^3$ nm/s, $\Delta F = (36 \pm 7) \cdot 10^{-3}$ mN$\}$. The blue curve is a fit with equation 7 giving $n = 0.30 \pm 0.02$.

$$F = Av^n, \tag{7}$$

This model also fits reasonably our data (blue curve in Figure 6(b)), with an exponent $n = 0.30 \pm 0.02$ close to the reported value of $1/3$. Therefore, these measurements of the friction force over two decades of shearing velocities allow us to unambiguously reject a description of the friction kinetics by an Arrhenius law, but not to discriminate between the modified Arrhenius law and the empirical power-law.

4 Conclusions

In this paper, we have presented proof-of-concept experiments for a new methodology to measure friction in the boundary lubrication regime with a SFB. By applying simultaneous normal and lateral motions to the surfaces, the friction-load relationship can be measured more precisely, comprehensively and rapidly. The quality achieved opens the way to more quantitative investigations to relate friction, load, contact area, adhesion and shearing velocity, while the efficiency and the versatility of the method allow for efficient probing of various physico-chemical systems. Using ionic liquids as a proof-of-concept, we have measured the phenomenon of quantized friction with an unprecedented resolution. Contrary to the existing studies in the area, we have found (i) a liquid-like friction behavior; (ii) a variation of the kinetic friction force with the applied load that is not simply linear, but can be quantitatively described by two additive contributions proportional to the load and to the contact area; (iii) a dynamics over two decades of shearing velocities that does not obey a simple Arrhenius law, appealing for more sophisticated models of friction kinetics. Furthermore, we have observed that humidity can improve the lubrication performances of ionic liquid, by increasing the resistance of the layers to be squeezed-out and so extending the range of loads in which the liquid behaves as a superlubricant.

The results presented in this study raise a number of questions, listed below, that would require dedicated experimental investigations.

- **Does the increase of mica surface charge with humidity explain the amplification of the ion density oscillation?** This aspect could be specifically addressed by performing measurements with conductive surfaces, which surface potential can be controlled externally[28,79–81].

- **Can the relative orientation of the mica surfaces induce a transition from a solid-like to a liquid-like friction behavior also for ionic liquids?** This hypothesis could be verified by measuring the friction behavior while varying systematically the twist angle between the mica surfaces.

- **Should friction kinetics across ionic liquids be described by a thermally-activated process, or by a shear-thinning rheology, or another approach?** The different models could be discriminated by exploring the dynamics over a wider range of shearing velocities to identify or not a spinodal transition, and by performing friction measurements at different temperatures.

- **Is the variability on the lateral force measurement when changing the contact spot correlated to the presence of large domains of uniform orientation on the surfaces?** This scenario could be tested by combining X-ray scattering and friction measurements in a modified SFA/SFB[40,82,83].

Conflicts of interest

There are no conflicts to declare.

Acknowledgements

S.P. and R.L. are supported by The Leverhulme Trust (RPG-2015-328) and the ERC (under Starting Grant No. 676861,

LIQUISWITCH). R.L. is supported by the EPA Cephalosporin Junior Research Fellowship and Linacre College (University of Oxford).

References

1 F. P. Bowden and D. Tabor, *The Friction and Lubrication of Solids*, Oxford University Press, 1950.

2 *Fundamentals of Friction and Wear on the Nanoscale (Second Edition)*, ed. E. Gnecco and E. Meyer, Springer, 2015.

3 R. Lhermerout, C. Diederichs and S. Perkin, *Lubricants*, 2018, **6**, 1–12.

4 R. G. Horn, D. F. Evans and B. W. Ninham, *J. Phys. Chem.*, 1988, **92**, 3531–3537.

5 R. Atkin and G. G. Warr, *J. Phys. Chem. C*, 2007, **111**, 5162–5168.

6 I. Bou-Malham and L. Bureau, *Soft Matter*, 2010, **6**, 4062–4065.

7 S. Perkin, T. Albrecht and J. Klein, *Phys. Chem. Chem. Phys.*, 2010, **12**, 1243–1247.

8 K. Ueno, M. Kasuya, M. Watanabe, M. Mizukami and K. Kurihara, *Phys. Chem. Chem. Phys.*, 2010, **12**, 4066–4071.

9 X. Zhang, Y.-X. Zhong, J.-W. Yan, Y.-Z. Su, M. Zhang and B.-W. Mao, *Chem. Commun.*, 2012, **48**, 582–584.

10 J. Hoth, F. Hausen, M. H. Müser and R. Bennewitz, *J. Phys. Condens. Matter*, 2014, **26**, 284110.

11 H.-W. Cheng, P. Stock, B. Moeremans, T. Baimpos, X. Banquy, F. U. Renner and M. Valtiner, *Adv. Mater. Interfaces*, 2015, **2**, 1500159–n/a.

12 L. Garcia, L. Jacquot, E. Charlaix and B. Cross, *Faraday Discuss.*, 2017, **206**, 443–457.

13 O. Werzer, E. D. Cranston, G. G. Warr, R. Atkin and M. W. Rutland, *Phys. Chem. Chem. Phys.*, 2012, **14**, 5147–5152.

14 A. Elbourne, J. Sweeney, G. B. Webber, E. J. Wanless, G. G. Warr, M. W. Rutland and R. Atkin, *Chem. Commun.*, 2013, **49**, 6797–6799.

15 A. M. Smith, K. R. J. Lovelock, N. N. Gosvami, T. Welton and S. Perkin, *Phys. Chem. Chem. Phys.*, 2013, **15**, 15317–15320.

16 J. Sweeney, G. B. Webber, M. W. Rutland and R. Atkin, *Phys. Chem. Chem. Phys.*, 2014, **16**, 16651–16658.

17 A. M. Smith, M. A. Parkes and S. Perkin, *J. Phys. Chem. Lett.*, 2014, **5**, 4032–4037.

18 N. Hjalmarsson, R. Atkin and M. W. Rutland, *Phys. Chem. Chem. Phys.*, 2016, **18**, 9232–9239.

19 J. N. Israelachvili, *Intermolecular and Surface Forces (Third Edition)*, Academic Press, 2011.

20 J. Klein and E. Kumacheva, *J. Chem. Phys.*, 1998, **108**, 6996–7009.

21 S. Perkin, L. Chai, N. Kampf, U. Raviv, W. Briscoe, I. Dunlop, S. Titmuss, M. Seo, E. Kumacheva and J. Klein, *Langmuir*, 2006, **22**, 6142–6152.

22 R. Lhermerout and S. Perkin, *Phys. Rev. Fluids*, 2018, **3**, 014201.

23 R. Lhermerout and S. Perkin, (to be published).

24 C. J. Rao, K. A. Venkatesan, B. Tata, K. Nagarajan, T. Srinivasan and P. Vasudeva Rao, *Radiat. Phys. Chem.*, 2011, **80**, 643 – 649.

25 R. M. Espinosa-Marzal, A. Arcifa, A. Rossi and N. D. Spencer, *J. Phys. Chem. C*, 2014, **118**, 6491–6503.

26 J. N. Israelachvili, *J. Colloid Interface Sci.*, 1973, **44**, 259 – 272.

27 K. A. Schwenzfeier, A. Erbe, P. Bilotto, M. Lengauer, C. Merola, H.-W. Cheng, L. L. E. Mears and M. Valtiner, *Rev. Sci. Instrum.*, 2019, **90**, 043908.

28 M. A. Gebbie, M. Valtiner, X. Banquy, E. T. Fox, W. A. Henderson and J. N. Israelachvili, *PNAS*, 2013, **110**, 9674–9679.

29 M. A. Gebbie, H. A. Dobbs, M. Valtiner and J. N. Israelachvili, *PNAS*, 2015, **112**, 7432–7437.

30 A. M. Smith, A. A. Lee and S. Perkin, *J. Phys. Chem. Lett.*, 2016, **7**, 2157–2163.

31 N. Hjalmarsson, R. Atkin and M. W. Rutland, *Chem. Commun.*, 2017, **53**, 647–650.

32 J. Comtet, A. Nigues, V. Kaiser, B. Coasne, L. Bocquet and A. Siria, *Nat. Mater.*, 2017, **16**, 634–639.

33 A. A. Lee, C. S. Perez-Martinez, A. M. Smith and S. Perkin, *Faraday Discuss.*, 2017, **199**, 239–259.

34 A. A. Lee, C. S. Perez-Martinez, A. M. Smith and S. Perkin, *Phys. Rev. Lett.*, 2017, **119**, 026002.

35 A. Crespo, D. Mazuyer, N. Morgado, A. Tonck, J.-M. Georges and J. Cayer-Barrioz, *Tribol. Lett.*, 2017, **65**, 138.

36 R. Lhermerout, C. Diederichs, S. Sinha, K. Porfyrakis and S. Perkin, *J. Phys. Chem. B*, 2019, **123**, 310–316.

37 M. L. Gee, P. M. McGuiggan, J. N. Israelachvili and A. M. Homola, *J. Chem. Phys.*, 1990, **93**, 1895–1906.

38 H. Yoshizawa, P. McGuiggan and J. Israelachvili, *Science*, 1993, **259**, 1305–1308.

39 S. Yamada and J. Israelachvili, *J. Phys. Chem. B*, 1998, **102**, 234–244.

40 Y. Golan, A. Martin-Herranz, Y. Li, C. R. Safinya and J. Israelachvili, *Phys. Rev. Lett.*, 2001, **86**, 1263–1266.

41 C. Drummond, N. Alcantar and J. Israelachvili, *Phys. Rev. E*, 2002, **66**, 011705.

42 R. M. Espinosa-Marzal, A. Arcifa, A. Rossi and N. D. Spencer, *J. Phys. Chem. Lett.*, 2014, **5**, 179–184.

43 J. Gao, W. D. Luedtke and U. Landman, *J. Phys. Chem. B*, 1998, **102**, 5033–5037.

44 A. Socoliuc, E. Gnecco, S. Maier, O. Pfeiffer, A. Baratoff, R. Bennewitz and E. Meyer, *Science*, 2006, **313**, 207–210.

45 P. A. Johnson, H. Savage, M. Knuth, J. Gomberg and C. Marone, *Nature*, 2008, **451**, 57.

46 R. Capozza, A. Vanossi, A. Vezzani and S. Zapperi, *Phys. Rev. Lett.*, 2009, **103**, 085502.

47 F. Giacco, E. Lippiello and M. P. Ciamarra, *Phys. Rev. E*, 2012, **86**, 016110.

48 H. Lastakowski, J.-C. Géminard and V. Vidal, *Sci. Rep.*, 2015, **5**, 13455.

49 B. V. Derjaguin, V. M. Muller and Y. P. Toporov, *J. Colloid Interface Sci.*, 1975, **53**, 314 – 326.

50 R. G. Horn, J. N. Israelachvili and F. Pribac, *J. Colloid Interface Sci.*, 1987, **115**, 480 – 492.

51 D. Maugis, *J. Colloid Interface Sci.*, 1992, **150**, 243 – 269.

52 D. S. Grierson, E. E. Flater and R. W. Carpick, *J. Adhes. Sci. Technol.*, 2005, **19**, 291–311.

53 A. M. Smith, A. A. Lee and S. Perkin, *Phys. Rev. Lett.*, 2017, **118**, 096002.

54 R. Hayes, S. Z. El Abedin and R. Atkin, *J. Phys. Chem. B*, 2009, **113**, 7049–7052.

55 B. V. Derjaguin, *Wear*, 1988, **128**, 19 – 27.

56 E. Kumacheva and J. Klein, *J. Chem. Phys.*, 1998, **108**, 7010–7022.

57 A. Berman, C. Drummond and J. Israelachvili, *Tribol. Lett.*, 1998, **4**, 95.

58 D. Gourdon and J. N. Israelachvili, *Phys. Rev. E*, 2003, **68**, 021602.

59 A. M. Homola, J. N. Israelachvili, M. L. Gee and P. M. McGuiggan, *J. Tribol.*, 1989, **111**, 675 – 682.

60 A. M. Homola, J. N. Israelachvili, P. M. McGuiggan and M. L. Gee, *Wear*, 1990, **136**, 65 – 83.

61 R. W. Carpick, N. Agraït, D. F. Ogletree and M. Salmeron, *Langmuir*, 1996, **12**, 3334–3340.

62 G. Bogdanovic, F. Tiberg and M. W. Rutland, *Langmuir*, 2001, **17**, 5911–5916.

63 M. Lessel, P. Loskill, F. Hausen, N. N. Gosvami, R. Bennewitz and K. Jacobs, *Phys. Rev. Lett.*, 2013, **111**, 035502.

64 J. N. Israelachvili, Y.-L. Chen and H. Yoshizawa, *J. Adhes. Sci. Technol.*, 1994, **8**, 1231–1249.

65 O. Y. Fajardo, F. Bresme, A. A. Kornyshev and M. Urbakh, *ACS Nano*, 2017, **11**, 6825–6831.

66 B. J. Briscoe, D. C. B. Evans and D. Tabor, *Proc. R. Soc. A*, 1982, **380**, 389–407.

67 E. Gnecco, R. Bennewitz, T. Gyalog, C. Loppacher, M. Bammerlin, E. Meyer and H.-J. Güntherodt, *Phys. Rev. Lett.*, 2000, **84**, 1172–1175.

68 M. He, A. Szuchmacher Blum, G. Overney and R. M. Overney, *Phys. Rev. Lett.*, 2002, **88**, 154302.

69 L. Ma, A. Gaisinskaya-Kipnis, N. Kampf and J. Klein, *Nat. Commun.*, 2015, **6**,.

70 Y. Sang, M. Dubé and M. Grant, *Phys. Rev. Lett.*, 2001, **87**, 174301.

71 E. Riedo, E. Gnecco, R. Bennewitz, E. Meyer and H. Brune, *Phys. Rev. Lett.*, 2003, **91**, 084502.

72 P. Reimann and M. Evstigneev, *New J. Phys.*, 2005, **7**, 25–25.

73 H.-W. Hu, G. A. Carson and S. Granick, *Phys. Rev. Lett.*, 1991, **66**, 2758–2761.

74 P. A. Thompson, G. S. Grest and M. O. Robbins, *Phys. Rev. Lett.*, 1992, **68**, 3448–3451.

75 M. Urbakh, L. Daikhin and J. Klafter, *Phys. Rev. E*, 1995, **51**, 2137–2141.

76 A. Brodsky, *Int. J. Mod. Phys. A*, 1998, **12**, 167–175.

77 S. T. Cui, C. McCabe, P. T. Cummings and H. D. Cochran, *J. Chem. Phys.*, 2003, **118**, 8941–8944.

78 M. Otsuki, *J. Phys. Soc. Jpn.*, 2008, **77**, 054002.

79 J. Sweeney, F. Hausen, R. Hayes, G. B. Webber, F. Endres, M. W. Rutland, R. Bennewitz and R. Atkin, *Phys. Rev. Lett.*, 2012, **109**, 155502.

80 R. Tivony and J. Klein, *Faraday Discuss.*, 2017, **199**, 261–277.

81 C. D. van Engers, M. Balabajew, A. Southam and S. Perkin, *Rev. Sci. Instrum.*, 2018, **89**, 123901.

82 S. H. Idziak, C. R. Safinya, R. S. Hill, K. E. Kraiser, M. Ruths, H. E. Warriner, S. Steinberg, K. S. Liang and J. N. Israelachvili, *Science*, 1994, **264**, 1915–1918.

83 P. Kékicheff, J. Iss, P. Fontaine and A. Johner, *Phys. Rev. Lett.*, 2018, **120**, 118001.